

Enhanced Aggregation of Alginate-Coated Iron Oxide (Hematite) Nanoparticles in the Presence of Calcium, Strontium, and Barium Cations

Kai Loon Chen,[†] Steven E. Mylon,[‡] and Menachem Elimelech^{*,†}

Department of Chemical Engineering, Environmental Engineering Program, Yale University, New Haven, Connecticut 06520-8286, and Department of Chemistry, Lafayette College, Easton, Pennsylvania 18042-1782

Received December 27, 2006. In Final Form: March 3, 2007

Early-stage aggregation kinetics studies of alginate-coated hematite nanoparticles in solutions containing alkaline-earth metal cations revealed enhanced aggregation rates in the presence of Ca²⁺, Sr²⁺, and Ba²⁺, but not with Mg²⁺. Transmission electron microscopy (TEM) imaging of the aggregates provided evidence that alginate gel formation was essential for enhanced aggregation to occur. Dynamic light scattering (DLS) aggregation results clearly indicated that a much lower concentration of Ba²⁺ compared to Ca²⁺ and Sr²⁺ was required to achieve a similar degree of enhanced aggregation in each system. To elucidate the relationship between the alginate's affinities for divalent cations and the enhanced aggregation of the alginate-coated hematite nanoparticles, atomic force microscopy (AFM) was employed to probe the interaction forces between alginate-coated hematite surfaces under the solution chemistries used for the aggregation study. Maximum adhesion forces, maximum pull-off distances, and the work of adhesion were used as indicators to gauge the alginate's affinity for the divalent cations and the resulting attractive interactions between alginate-coated hematite nanoparticles. The results showed that alginate had higher affinity for Ba²⁺ than either Sr²⁺ or Ca²⁺. This same trend was consistent with the cation concentrations required for comparable enhanced aggregation kinetics, suggesting that the rate of alginate gel formation controls the enhanced aggregation kinetics. An aggregation mechanism incorporating the gelation of alginate is proposed to explain the accelerated aggregate growth in the presence of Ca²⁺, Sr²⁺, and Ba²⁺.

1. Introduction

The classic Derjaguin–Landau–Verwey–Overbeek (DLVO) theory of colloidal stability has been universally used to explain the aggregation behavior of charged colloidal particles in the presence of simple electrolytes.^{1,2} In such scenarios, the stability of the colloidal particles is controlled by the interplay between the electrostatic and van der Waals interactions. However, the presence of polyelectrolytes introduces greater complexity to the system.^{3,4} There is a dual nature to polyelectrolyte adsorption onto colloidal particles. Polyelectrolytes can alter colloidal surface properties and can often engender steric repulsion between the particles.^{5,6} Additionally, depending on the type of polyelectrolyte and solution chemistry, polyelectrolytes may bridge colloidal particles together.^{7,8} Thus, the presence of polyelectrolytes can either retard or enhance the aggregate growth rates.

Suspensions comprising colloidal particles and polyelectrolytes are often encountered in biomedical, environmental, and industrial applications.^{9,10} Alginates represent one of the common poly-

electrolytes found in many of these systems. Produced by brown algae as well as some bacteria,^{11,12} alginates are naturally occurring linear polysaccharides consisting of 1,4-linked β -D-mannuronic (M) and α -L-guluronic (G) acid residues. These block copolymers are made up of M-blocks, G-blocks, and MG-blocks. The prevalence and sequence of the block types control the chemistry of alginates in solution and are highly dependent on the source of the alginates.¹³

It is widely recognized that most divalent cations are able to complex to the G-blocks from two alginate polymers, forming a cooperative “egg-box structure”, thereby linking the two polymers.^{11,14–18} The cross-linking of numerous alginate polymers at multiple sites along the polymer backbone results in alginate gel formation. However, monovalent cations (e.g., Na⁺ and K⁺) and magnesium do not induce alginate gel formation.^{11,19,20} In a recent study, Mørch et al.²⁰ reported that while calcium, strontium, and barium ions complex at the G-blocks, they may

* To whom correspondence should be addressed. E-mail: menachem.elimelech@yale.edu. Phone: (203) 432-2789.

[†] Yale University.

[‡] Lafayette College.

(1) Verwey, E. J. W.; Overbeek, J. T. G. *Theory of the Stability of Lyophobic Colloids*; Elsevier: Amsterdam, 1948.

(2) Derjaguin, B. V.; Landau, L. D. *Acta Physicochim. URSS* **1941**, *14*, 733–762.

(3) Elimelech, M.; Gregory, J.; Jia, X.; Williams, R. A. *Particle Deposition and Aggregation: Measurement, Modelling and Simulation*; Butterworth-Heinemann: Oxford, England, 1995.

(4) Israelachvili, J. *Intermolecular and Surface Forces*; Academic Press: London, England, 1991.

(5) Tiller, C. L.; O'Melia, C. R. *Colloids Surf., A* **1993**, *73*, 89–102.

(6) Stenkamp, V. S.; McGuiggan, P.; Berg, J. C. *Langmuir* **2001**, *17* (3), 637–651.

(7) Gregory, J. *J. Colloid Interface Sci.* **1973**, *42* (2), 448–456.

(8) Braem, A. D.; Campos-Teran, J.; Lindman, B. *Langmuir* **2004**, *20* (15), 6407–6413.

(9) Yu, W. L.; Bouyer, F.; Borkovec, M. *J. Colloid Interface Sci.* **2001**, *241* (2), 392–399.

(10) Mosley, L. M.; Hunter, K. A.; Ducker, W. A. *Environ. Sci. Technol.* **2003**, *37* (15), 3303–3308.

(11) Gombotz, W. R.; Wee, S. F. *Adv. Drug Delivery Rev.* **1998**, *31* (3), 267–285.

(12) Lattner, D.; Flemming, H. C.; Mayer, C. *Int. J. Biol. Macromol.* **2003**, *33* (1–3), 81–88.

(13) Siew, C. K.; Williams, P. A.; Young, N. W. G. *Biomacromolecules* **2005**, *6* (2), 963–969.

(14) Vold, I. M. N.; Kristiansen, K. A.; Christensen, B. E. *Biomacromolecules* **2006**, *7* (7), 2136–2146.

(15) Davis, T. A.; Llanes, F.; Volesky, B.; Mucci, A. *Environ. Sci. Technol.* **2003**, *37* (2), 261–267.

(16) Emmerichs, N.; Wingender, J.; Flemming, H. C.; Mayer, C. *Int. J. Biol. Macromol.* **2004**, *34* (1–2), 73–79.

(17) Smidsrød, O.; Haug, A. *Acta Chem. Scand.* **1965**, *19* (2), 329–&.

(18) Haug, A.; Smidsrød, O. *Acta Chem. Scand.* **1965**, *19* (2), 341–&.

(19) Davis, T. A.; Volesky, B.; Mucci, A. *Water Res.* **2003**, *37* (18), 4311–4330.

(20) Mørch, Y. A.; Donati, I.; Strand, B. L.; Skjåk-Bræk, G. *Biomacromolecules* **2006**, *7* (5), 1471–1480.

also form complexes at M-blocks and MG-blocks, albeit to different extents. In light of the differences in the nature of divalent cation complexation, the strength and structural stability of the alginate gel vary with both the composition of the alginate polymers and the divalent cations present in the solution.^{15,19,20}

Because alginates are nontoxic, biodegradable, and relatively nonimmunogenic in cases where G-blocks are predominant,^{14,21} they are widely utilized in biomedical applications. For example, calcium cations are usually employed to prepare alginate hydrogels and microbeads for cell encapsulation and drug delivery purposes.^{20,22–25} In addition to calcium, strontium and barium are two possible divalent cations suitable for use in these applications.²⁰ Systems comprising alginate and colloidal particles have also been proposed for biomedical applications. One example of such systems is prepared by mixing colloidal silica in a sodium alginate solution prior to gelation in the presence of calcium ions. The result of this preparation is a stronger alginate microcapsule that can be used to encapsulate cells or biomolecules.²⁶ In another application, Shen et al.²⁷ prepared suspensions of magnetic iron oxide nanoparticles in alginate solution to synthesize alginate microcapsules for use as contrast agents in magnetic resonance imaging (MRI). In the field of optoelectronics, silver–gold composite colloids have been synthesized in alginate solutions so that the polyelectrolytes can act as protective agents to prevent particles from coalescing.²⁸ Alginate has also been suggested to be an effective flocculating agent for solids removal in effluent treatment processes.²⁹

In our earlier paper,³⁰ we investigated the early-stage aggregation kinetics of alginate-coated iron oxide (hematite) nanoparticles in the presence of Na⁺, Mg²⁺, and Ca²⁺ ions. Our results suggested that alginate gel formation leads to enhanced aggregate growth rates in the presence of higher Ca²⁺ concentrations. These apparent rates were even greater than diffusion-limited aggregation rates observed in solutions where the Na⁺ and Mg²⁺ concentrations exceeded the critical coagulation concentrations (CCCs). This work stopped short of measuring the interaction forces responsible for the aggregation of the alginate-coated hematite nanoparticles. By employing atomic force microscopy (AFM), we can provide insights into the interactions between the nanoparticles,^{8,10,31} which may allow a better understanding of the enhanced aggregation process of the alginate-coated hematite nanoparticles.

The objective of this study is to broaden our understanding of the role of alginates in the presence of alkaline-earth metal divalent cations on the enhanced aggregation of alginate-coated hematite nanoparticles. We accomplish this by determining the influence of Sr²⁺ and Ba²⁺ cations on the nanoparticle aggregation

kinetics and comparing the observed behavior with our previous results obtained in the presence of Ca²⁺ and Mg²⁺. We also included transmission electron microscopy (TEM) imaging and AFM force measurements in this work to complement the aggregation kinetics study through dynamic light scattering (DLS). TEM imaging of the aggregate structures verified the formation of alginate gel that bridged the hematite nanoparticles and aggregates under solution conditions that led to enhanced aggregation. Furthermore, AFM force measurements indicated that the propensity of alginate gel formation in the presence of different divalent cations is strongly correlated with the degree of enhanced aggregation determined from DLS. On the basis of multiple lines of evidence from the three experimental components of this work, we proposed a detailed aggregation mechanism for accelerated aggregate growth in the presence of Ca²⁺, Sr²⁺, and Ba²⁺.

2. Materials and Methods

2.1. Alginate Source and Characterization. Sodium alginate (A2158, Sigma-Aldrich, St. Louis, MO) extracted from the brown algae species *Macrocystis pyrifera* was used in this study. According to the supplier, the alginate comprises approximately 61% mannuronic acid and 39% guluronic acid and has a molecular weight ranging from 12 to 80 kDa. Its total organic carbon (TOC) content was determined to be about 31% of its dry mass by high-temperature oxidation at 680 °C (TOC-V CSH, Shimadzu, Kyoto, Japan). We had previously determined the carboxylic acidity of this alginate to be 2.7 meq/g of alginate through potentiometric titration.³⁰

2.2. Preparation and Characterization of Hematite Nanoparticles. Hematite nanoparticles were synthesized through forced hydrolysis of FeCl₃,³² as described in our previous paper.³³ Hematite synthesis was confirmed through X-ray powder diffraction analysis using a Scintag DMS 2000 with Cu K α radiation. In short, dried material was pulverized to a fine powder. To about 20 mg of powder were added 100 μ L of amyl acetate (Sigma-Aldrich) and 5 μ L of collodion solution (Sigma-Aldrich). Several drops of the resulting suspension were allowed to dry on a glass slide. Scans were made from $2\theta = 20^\circ$ to $2\theta = 80^\circ$ at $1^\circ/\text{min}$ using filtered Cu radiation and a monochromator. Cu K α_2 peaks were stripped mathematically. Diffraction maxima were determined by Scintag's Peakfinder software and compared to those of relevant materials listed in Scintag's database. For each sample, the experimental diffraction pattern matched that for synthetic hematite exactly.

Through gravimetric analysis, the hematite stock concentration was found to be 5.5 g/L. The hydrodynamic radius of the hematite nanoparticles was determined to be 37.4 ± 1.1 nm (20 measurements) through DLS (ALV-5000, Langen, Germany), which is consistent with the mean diameter determined from TEM imaging. TEM imaging also showed that the nanoparticles were monodisperse and mostly spherical with slight angularities. Assuming the nanoparticles to be spherical with a diameter of 75 nm and the hematite specific gravity to be 5.3, the stock suspension was calculated to have a concentration of 4.5×10^{12} particles/mL.

The electrophoretic mobilities of the hematite nanoparticles were measured (ZetaPALS, Brookhaven Instruments Corp., Holtsville, NY) over a range of pH conditions in the presence of 10 mM NaCl to determine their isoelectric point (IEP). Five electrophoretic mobility measurements were taken for each sample, and measurements were conducted for at least three independent samples at each pH. The ζ potentials of the nanoparticles were obtained by converting the average values of the electrophoretic mobilities using the tabulated values provided by Ottewill and Shaw.³⁴

(21) Bu, H. T.; Kjoniksen, A. L.; Knudsen, K. D.; Nystrom, B. *Biomacromolecules* **2004**, *5* (4), 1470–1479.

(22) LeRoux, M. A.; Guilak, F.; Setton, L. A. *J. Biomed. Mater. Res.* **1999**, *47* (1), 46–53.

(23) Rowley, J. A.; Madlambayan, G.; Mooney, D. J. *Biomaterials* **1999**, *20* (1), 45–53.

(24) Hoffman, A. S. *Adv. Drug Delivery Rev.* **2002**, *54* (1), 3–12.

(25) De Boissesson, M. R.; Leonard, M.; Hubert, P.; Marchal, P.; Stequert, A.; Castel, C.; Favre, E.; Dellacherie, E. *J. Colloid Interface Sci.* **2004**, *273* (1), 131–139.

(26) Coradin, T.; Nassif, N.; Livage, J. *Appl. Microbiol. Biotechnol.* **2003**, *61* (5–6), 429–434.

(27) Shen, F.; Poncet-Legrand, C.; Somers, S.; Slade, A.; Yip, C.; Duft, A. M.; Winnik, F. M.; Chang, P. L. *Biotechnol. Bioeng.* **2003**, *83* (3), 282–292.

(28) Sato, T.; Kuroda, S.; Takami, A.; Yonezawa, Y.; Hada, H. *Appl. Organomet. Chem.* **1991**, *5* (4), 261–268.

(29) Tripathy, T.; Pandey, S. R.; Karmakar, N. C.; Bhagat, R. P.; Singh, R. P. *Eur. Polym. J.* **1999**, *35* (11), 2057–2072.

(30) Chen, K. L.; Mylon, S. E.; Elimelech, M. *Environ. Sci. Technol.* **2006**, *40* (5), 1516–1523.

(31) Abu-Lail, N. I.; Camesano, T. A. *J. Microsc. (Oxford)* **2003**, *212*, 217–238.

(32) Matijević, E.; Scheiner, P. *J. Colloid Interface Sci.* **1978**, *63* (3), 509–524.

(33) Mylon, S. E.; Chen, K. L.; Elimelech, M. *Langmuir* **2004**, *20* (21), 9000–9006.

(34) Ottewill, R. H.; Shaw, J. N. *J. Electroanal. Chem.* **1972**, *37* (June), 133–142.

The alginate-coated hematite nanoparticles were prepared by diluting the hematite stock suspension into a sodium alginate solution and leaving the mixture aside for at least a month to allow for extensive adsorption to take place. More details on the preparation protocol are provided in our previous paper.³⁰ Since we were not able to remove the unadsorbed alginate, the alginate-coated hematite stock suspension also contained dissolved alginate. For this stock suspension, we calculated the alginate-coated nanoparticle concentration to be 1.0×10^{12} particles/mL. By centrifuging a sample of the stock solution and measuring the TOC of the supernatant, we determined the dissolved (unadsorbed) alginate content in the stock solution to be 494 mg/L. Through mass balance, the degree of adsorption was found to be 42.5 mg of alginate/g of hematite. It is worthwhile to mention that the alginate-coated hematite nanoparticles used for the new aggregation experiments conducted in the presence of SrCl₂ and BaCl₂ belong to the same batch of coated nanoparticles used in our previous study.³⁰

2.3. Electrolyte Solutions. The monovalent (NaCl) and divalent (MgCl₂, CaCl₂, SrCl₂, and BaCl₂) electrolyte stock solutions employed for all experiments were prepared from salts purchased from Fisher Scientific (ACS reagent grade) and filtered with 0.1 μm filters (Anotop 25, Whatman, Middlesex, U.K.) before use. For all experiments, the pH of the test solutions was adjusted to 5.2 ± 0.1 with HCl, under which the alginate-coated hematite nanoparticles were stable at low ionic strengths.

2.4. Hematite Nanoparticle Aggregation. The early-stage aggregation kinetics of the alginate-coated hematite nanoparticles in the presence of monovalent and divalent electrolytes were derived through time-resolved DLS. Details on the DLS setup, aggregation experiments, and determination of aggregation kinetics are given below.

2.4.1. Dynamic Light Scattering. The time-resolved DLS measurements were performed with a multidetector light scattering unit (ALV-5000, Langen, Germany). This instrument utilizes a Nd:vanadate laser (Verdi V2, Coherent, Santa Clara, CA) operating at a wavelength of 532 nm. Additional details on this instrument are provided in our earlier papers.^{30,33}

For the aggregation experiments in the presence of CaCl₂, SrCl₂, and BaCl₂ electrolytes, the alginate stock suspension was diluted 13200 times in deionized water (Barnstead), resulting in a nanoparticle concentration of 7.6×10^7 particles/mL and a dissolved alginate concentration of 37.4 μg/L. In the presence of NaCl and MgCl₂ electrolytes, the nanoparticle and dissolved alginate concentrations employed for the aggregation experiments were twice those used in the presence of the other divalent electrolytes. For each aggregation experiment, a new glass vial (Supelco, Bellefonte, PA) was used to hold 2 mL of the dilute alginate-coated hematite nanoparticle suspension. The glass vials had been soaked overnight in cleaning solution (Extran MA01, Merck KGaA, Darmstadt, Germany), rinsed in excess deionized water, and oven-dried under dust-free conditions before use. To induce aggregation of the nanoparticles, a premeasured volume of electrolyte stock solution was added to the vial containing the diluted nanoparticle suspension. The vial was then briefly vortexed (Mini Vortexer, Fisher Scientific) to ensure a well-mixed suspension and quickly inserted into the vat of the light scattering unit. DLS measurements were started immediately after the vial was secure in the index-matching vat. All measurements were carried out at a room temperature of 23 °C.

For each DLS measurement, scattered light was collected by the detector positioned at an angle of 90°. Each autocorrelation function was accumulated for 15 s, and the intensity-weighted hydrodynamic radius of the particle aggregates was determined with second-order cumulant analysis (ALV software). The measurements were carried out for a time period of between 20 min and 4 h to allow for about a 30% increase in the hydrodynamic radius.

2.4.2. Determination of Aggregation Kinetics. In this study, we are interested in the early-stage aggregation kinetics, which can be described by the initial rate of doublet formation as shown in eq 1,³

$$\left(\frac{dN_2(t)}{dt}\right)_{t \rightarrow 0} = \frac{1}{2}k_{11}N_0^2 \quad (1)$$

where $N_2(t)$ is the concentration of doublets as a function of time t , N_0 is the initial primary particle concentration, and k_{11} is the absolute aggregation rate constant. Within the Rayleigh–Gans–Debye (RGD) approximation, k_{11} can be derived from^{30,35,36}

$$\frac{1}{r_h(0,q)} \left(\frac{dr_h(t,q)}{dt}\right)_{t \rightarrow 0} = k_{11}N_0 \left[1 + \frac{\sin(2aq)}{2aq}\right] \left(1 - \frac{1}{\delta}\right) \quad (2)$$

Here, q is the scattering vector defined as $(4\pi n/\lambda) \sin(\theta/2)$, where n is the refractive index of the medium, λ the wavelength of light, and θ the scattering angle. The hydrodynamic radius $r_h(t,q)$ is expressed as a function of t and q , a is the primary particle radius, and δ is the relative hydrodynamic radius of the doublet, which has been reported to be about 1.38.^{35,36} For each aggregation experiment, the derivative on the left-hand side of eq 2 is obtained through the linear least-squares regression analysis of the initial data points collected by DLS. To be consistent in the analysis, we ensured that the range of data points employed for analysis corresponds to an increase of the hydrodynamic radius to $1.3a$ and that the y intercept of the fitted line is within 3 nm in excess of a . Since all the other terms in eq 2 are known constants, k_{11} can be readily determined.

The inverse stability ratio $1/W$ was determined by normalizing the absolute aggregation rate constant determined at any electrolyte concentration to that obtained under favorable or diffusion-limited (fast) aggregation conditions, $(k_{11})_{\text{fast}}$, according to

$$\frac{1}{W} = \frac{k_{11}}{(k_{11})_{\text{fast}}} \quad (3)$$

The inverse stability ratio $1/W$ serves as an appropriate quantitative measure of the aggregation kinetics (or colloidal stability) of the nanoparticles at a particular solution chemistry in comparison to the aggregation kinetics controlled purely by diffusion.

2.4.3. TEM Imaging of Aggregates. Aggregate structures were observed by TEM after 3–4 h of aggregation. Details on the preparation and imaging protocol are described in our previous paper.³⁰

2.5. Interaction Force Measurement with AFM. The interaction forces between an alginate-coated hematite colloidal probe and an alginate-coated hematite substrate were measured with an AFM setup under similar solution chemistries employed in the aggregation experiments. The objective of the force measurements was to gain more insight into the nature of the interactions between the alginate-coated hematite nanoparticles in the presence of monovalent and various divalent electrolytes.

2.5.1. Preparation of the AFM Hematite Colloidal Probe. Micrometer-sized hematite particles were synthesized through the method described by Sugimoto and Sakata.³⁷ In this process, 100 mL of 5.4 M NaOH was slowly introduced into 110 mL of 2.0 M FeCl₃ solution contained in a 250 mL polypropylene bottle. The solution was shaken vigorously for approximately 10 min, before being aged in a preheated oven at 100 °C for 8 days. After aging, the solution was allowed to cool at room temperature. Once the freshly synthesized micrometer-sized hematite particles had settled to the bottom of the bottle, the particles were resuspended and washed in deionized water eight times before being stored at 4 °C.

To characterize the shape and size of the micrometer-sized hematite particles, they were observed through scanning electron microscopy (SEM). This was done by filtering a few drops of the particle stock suspension through a 0.2 μm membrane filter (Fisher Scientific) under vacuum, resulting in a cake layer of particles deposited on the membrane. The cake layer was then examined under an electron microscope (XL30 FEG ESEM, FEI). To characterize the surface charge of the particles, their electrophoretic mobilities were measured

(35) Holthoff, H.; Egelhaaf, S. U.; Borkovec, M.; Schurtenberger, P.; Sticher, H. *Langmuir* **1996**, *12* (23), 5541–5549.

(36) Kleimann, J.; Gehin-Delval, C.; Auweter, H.; Borkovec, M. *Langmuir* **2005**, *21* (8), 3688–3698.

(37) Sugimoto, T.; Sakata, K. *J. Colloid. Interface Sci.* **1992**, *152* (2), 587–590.

with the ZetaPALS over a range of pH conditions in a background solution of 10 mM NaCl to determine their IEP. Five electrophoretic mobility measurements were taken for each sample, and measurements were conducted for at least three independent samples under each pH condition. The ζ potentials of the micrometer-sized particles were calculated from the electrophoretic mobilities using the Smoluchowski equation.³

To prepare the hematite colloidal probe for AFM force measurements, 2.0 μL of micrometer-sized hematite stock suspension was left on a clean mica sheet. The mica sheet was gently blow-dried under a blanket of ultrapure argon gas, leaving the dried hematite particles deposited on the mica surface. Using a micromanipulator, a micrometer-sized hematite particle was glued to the end of a triangular tipless silicon nitride cantilever (NP-020, Veeco Probes, Santa Barbara, CA) with UV-curable glue (Norland Optical Adhesive, Norland Products, Inc., Cranbury, NJ). According to the manufacturer, the cantilever is 212 μm in length, with a spring constant of 0.06 N/m. All cantilevers used for the study were calibrated by Novascan Technologies, Inc. (Ames, IA) and were found to range between 0.056 and 0.075 N/m (seven cantilevers). The colloidal cantilever probe was oxidized in a UV–ozone chamber (BioForce Nanosciences, Inc., Ames, IA) for 20 min to remove any possible organic contaminants before use.

2.5.2. Hematite-Coated Quartz Substrate Preparation. Quartz microscope slides (Electron Microscopy Sciences, Hatfield, PA), about 1 mm thick, were cut into 15 mm square pieces. The cut slides were sonicated in acetone for 30 min and rinsed with deionized water, before undergoing another sonication in 2% Hellmanex II (Hellma GmbH & Co. KG, Müllheim, Germany) cleaning solution for 30 min. The slides were left to soak overnight in the cleaning solution, thoroughly rinsed with deionized water, blow-dried with ultrapure argon gas, and oxidized in a UV–ozone chamber for 20 min. Each cleaned slide was placed on a glass Petri dish, and 5.0 μL of hematite nanoparticle stock suspension was dropped onto its center. The Petri dishes were covered and left in the oven at 100 °C overnight. This resulted in a thin layer of hematite nanoparticles coating the center portion of the quartz slide surface. The hematite-coated quartz slides were oxidized in the UV–ozone chamber for 20 min before use. SEM imaging verified a complete coverage of the hematite nanoparticles on the quartz surface. This coverage will be further analyzed by AFM force measurements in section 3.3.1.

2.5.3. Determination of Interaction Forces by AFM. The force measurements were conducted using a Digital Instruments NanoScope IIIa MultiMode atomic force microscope (Veeco Metrology, Santa Barbara, CA). Each hematite-coated quartz slide was secured on the AFM piezoelectric scanner. The glass flow cell (MTFML, Veeco Probes) was rinsed with excess ethanol followed by deionized water and blow-dried with ultrapure argon gas before and after use. The hematite colloidal cantilever probe was mounted in the fluid cell, which was held in place over the coated quartz slide by two retaining springs.

For each series of experiments, deionized water was first slowly introduced into the flow cell with a syringe, and force measurements were taken between the bare hematite colloidal probe and hematite-coated quartz surface to check for sufficient coverage of the quartz surface with hematite nanoparticles. After this, an alginate solution with a concentration of 2.2 g/L and a pH of 5.2 was introduced into the liquid cell at a rate of 0.2 mL/min for 30 min using a syringe pump (KD Scientific Inc., Holliston, MA). Following this, the alginate stock solution was left stagnant in the liquid cell for 1 h to allow adequate alginate adsorption to take place on the hematite probe and the hematite-coated quartz surface. Adsorption occurs readily at pH 5.2 as the alginate and hematite are oppositely charged. Deionized water (adjusted to a pH of 5.2) was flushed through the liquid cell at 0.2 mL/min for 30 min to wash unadsorbed alginate from the system.

Each series of experiments consisted of two sets of measurements at two different electrolyte concentrations (100 and 200 mM for NaCl and 1 and 3 mM for divalent electrolytes), both containing 75 $\mu\text{g/L}$ alginate to simulate solution conditions of the aggregation experiments. For each electrolyte, a new set of hematite probe and

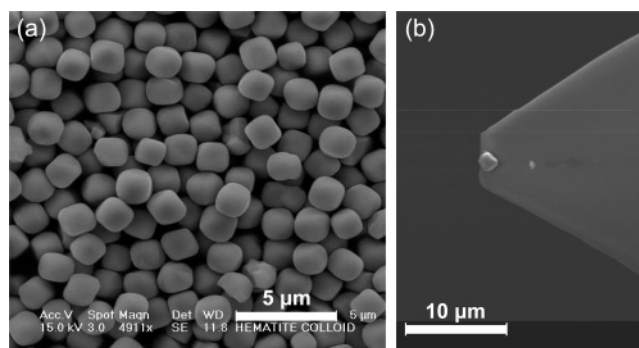


Figure 1. (a) SEM image of micrometer-sized hematite particles synthesized for employment as an AFM colloidal probe. (b) SEM image of a micrometer-sized hematite particle glued onto an AFM tipless cantilever.

hematite-coated quartz substrate was employed for force measurements. The electrolyte solutions were degassed through sonication prior to the experiments to prevent air bubble formation in the flow cell. A predetermined volume of alginate stock solution was added into the electrolyte solution just prior to its introduction into the flow cell to yield an alginate concentration of 75 $\mu\text{g/L}$. The solution with the lower electrolyte concentration was first passed through the liquid cell at 0.2 mL/min with the syringe pump for 30 min to ensure complete replacement of the deionized water. The solution was then left stagnant within the cell for 15 min for the adsorbed alginate to approach equilibrium. Force measurements were conducted between the alginate-coated surfaces in the presence of the electrolyte solution. Following this, the solution with higher electrolyte concentration, also containing 75 $\mu\text{g/L}$ alginate, was introduced into the flow cell using the same procedure, thereby displacing the electrolyte with the lower concentration. The solution was then left to equilibrate with the adsorbed alginate for 15 min. Force measurements were then taken under the new solution conditions.

For each solution chemistry, force measurements were taken at 5–6 different locations on the substrate, with at least 20 measurements at each location. For all measurements, the scan rate and ramp size were 0.49 Hz and 1.0 μm , respectively, thus resulting in an average cantilever approach and retract velocity of 0.98 $\mu\text{m/s}$. The maximum adhesion forces, maximum pull-off distances, and work of adhesion for all solution chemistries were compiled using Matlab (The MathWorks Inc., Natick, MA).

3. Results and Discussion

3.1. Characteristics of Hematite Nanoparticles and Micrometer-Sized Particles. TEM images of the synthesized bare hematite nanoparticles were presented in our previous paper.³³ They were observed to be monodisperse and mostly spherical, with a mean diameter of about 75 nm. SEM imaging of the micrometer-sized hematite particles revealed that they were reasonably monodisperse and slightly cubical with rounded edges and sides of about 1.7 μm (Figure 1a). Figure 1b presents the SEM image of a micrometer-sized hematite particle glued to the tip of the AFM cantilever to be used for force measurements.

The ζ potentials of the bare hematite nanoparticles and micrometer-sized particles in 10 mM NaCl solutions at 25 °C are presented as a function of pH in Figure 2. From Figure 2, the IEPs of the hematite nanoparticles and micrometer-sized particles are estimated to be 9.3 and 8.6, respectively, which are close to values reported elsewhere.^{38,39}

3.2. Aggregation Kinetics in the Presence of Monovalent and Divalent Cations. We have previously found the aggregation behavior of the alginate-coated hematite nanoparticles in the

(38) Pochard, I.; Denoyel, R.; Couchot, P.; Foissy, A. J. *Colloid Interface Sci.* **2002**, 255 (1), 27–35.

(39) Vermeer, A. W. P.; van Riemsdijk, W. H.; Koopal, L. K. *Langmuir* **1998**, 14 (10), 2810–2819.

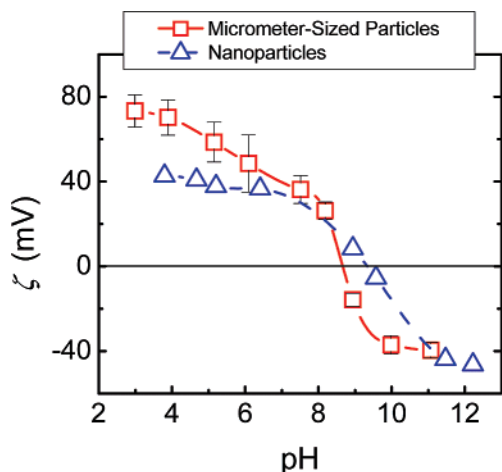


Figure 2. ζ potentials of hematite nanoparticles and micrometer-sized particles as a function of pH in the presence of 10 mM NaCl. The error bars represent standard deviations. All measurements were conducted at 25 °C. Bold and dashed lines are meant to guide the eye.

presence of NaCl and MgCl₂ to be consistent with the classic DLVO theory.³⁰ At low electrolyte concentrations, reaction-limited (slow) aggregation occurs since repulsive forces exist between the negatively charged alginate-coated nanoparticles. At electrolyte concentrations above the respective CCCs, diffusion-limited (fast) aggregation takes place as the surface charge on the alginate-coated nanoparticles is sufficiently screened to eliminate the energy barrier to aggregation. Using the DLS aggregation kinetics data and eq 2, we determined the absolute aggregation rate constants under diffusion-limited conditions, $(k_{11})_{\text{fast}}$, of the alginate-coated hematite nanoparticles in the presence of NaCl and MgCl₂ to be 6.9×10^{-18} and 8.1×10^{-18} m³/s, respectively.³⁰

In the presence of higher CaCl₂ electrolyte concentrations, we observed aggregate growth rates of up to an order of magnitude higher than rates observed under diffusion-limited aggregation conditions.³⁰ Through TEM imaging of the aggregate structures, we found that the enhanced aggregation in the presence of higher CaCl₂ concentrations involved the formation of an alginate gel that could bridge the alginate-coated hematite nanoparticles.³⁰ Since the enhanced aggregation mechanism is not simply governed by electrostatic destabilization, we introduced the apparent aggregation rate constant, k_{app} , in place of k_{11} in eq 2. Thus, k_{app} no longer describes the rate of doublet formation as in k_{11} , but serves as a general term to quantify the rate of aggregate growth without making any assumption about the aggregation mechanism. Similarly, we use the inverse stability ratio, $1/W$, to present the ratio of the aggregation rate constant under the studied solution chemistry to the diffusion-limited (fast) rate constant $(k_{11})_{\text{fast}}$:

$$\frac{1}{W} = \frac{k_{\text{app}}}{(k_{11})_{\text{fast}}} \quad (4)$$

In this study, the alginate-coated hematite nanoparticles were allowed to aggregate over a range of SrCl₂ and BaCl₂ concentrations at pH 5.2. The inverse stability ratios $1/W$ as functions of SrCl₂ and BaCl₂ concentrations are shown in Figure 3. Also included in Figure 3 are the inverse stability ratios of the alginate-coated hematite nanoparticles as functions of NaCl, MgCl₂, and CaCl₂ concentrations as determined in our previous study.³⁰ To derive the inverse stability ratios in the presence of CaCl₂, SrCl₂, and BaCl₂, $(k_{11})_{\text{fast}}$ obtained with NaCl (6.9×10^{-18} m³/s) was

used in eq 4. As observed, DLVO-type aggregation behavior in the presence of NaCl and MgCl₂ results in $1/W < 1$ in the reaction-limited regime and $1/W = 1$ in the diffusion-limited regime. At pH 5.2, the CCCs in the presence of NaCl and MgCl₂ are approximately 180 mM NaCl and 5 mM MgCl₂, respectively. The CCC in the presence of MgCl₂ is much lower than in the presence of NaCl because Mg²⁺ is more efficient in screening the charges of the alginate polyelectrolytes adsorbed on the hematite nanoparticle surface.⁴⁰

Enhanced aggregation rates are observed at higher concentrations of CaCl₂, SrCl₂, and BaCl₂, as indicated by $1/W$ values greater than 1. Specifically, in the presence of CaCl₂, SrCl₂, and BaCl₂ at concentrations higher than 2.9, 2.4, and 0.9 mM, respectively, the aggregate growth rate is faster than the growth rate that should occur under diffusion-limited conditions. At high enough concentrations of these electrolytes, we observed that the rate of aggregate growth can be 10 times that of the diffusion-limited aggregation rate (i.e., $1/W = 10$). Since enhanced aggregation was not observed in the presence of NaCl and MgCl₂, neither of which causes alginate gelation, the accelerated aggregate growth rates in the presence of CaCl₂, SrCl₂, and BaCl₂ are likely due to alginate gelation. This is verified through TEM imaging of the aggregate structures formed at higher CaCl₂, SrCl₂, and BaCl₂ concentrations, which revealed dispersed hematite nanoparticles and lower-order aggregates enmeshed within extended alginate gel networks.

Comparing the inverse stability ratio profiles among CaCl₂, SrCl₂, and BaCl₂ in Figure 3, the concentration of SrCl₂ required to achieve the same degree of enhanced aggregation is slightly lower than that required of CaCl₂. Likewise, a much lower concentration of BaCl₂ is required compared to that of SrCl₂ to attain equivalent enhanced aggregation kinetics. This may suggest a difference in the affinity of the alginate for the divalent cations and, hence, a difference in the propensity of alginate to undergo gelation in the presence of the cations. This affinity is verified through independent force measurements made between alginate-coated hematite surfaces using AFM as described in the following section.

Additional aggregation experiments were conducted on similarly prepared alginate-coated hematite nanoparticles, except that only 1 day was given for alginate adsorption on the hematite nanoparticles. It was also found that enhanced aggregation occurred at higher concentrations of CaCl₂, SrCl₂, and BaCl₂ (results not shown). A TEM image of a typical combined hematite–alginate gel aggregate in the presence of 6 mM SrCl₂ is presented in Figure 4. Similar aggregate structures in the presence of 6 mM CaCl₂ and 2 mM BaCl₂ were also observed (images not shown). These results suggest that adsorption of alginate onto hematite nanoparticles occurs in a reasonably short period of time.

3.3. Interaction Forces between Alginate-Coated Hematite Surfaces. To better understand the influence of the various divalent cations on the interactions of the alginate-coated hematite nanoparticles during aggregation, AFM measurements of the interaction forces between the alginate-coated hematite probe and substrate were conducted. The AFM force measurements were made using solution chemistries similar to those used in the aggregation experiments of the alginate-coated hematite nanoparticles.

3.3.1. Verification of Hematite Nanoparticle Coverage on the Quartz Surface. At the start of each series of AFM experiments, force measurements were conducted between the colloidal hematite probe and the pre-prepared hematite-coated quartz

(40) Stefansson, M. *Anal. Chem.* **1999**, *71* (13), 2373–2378.

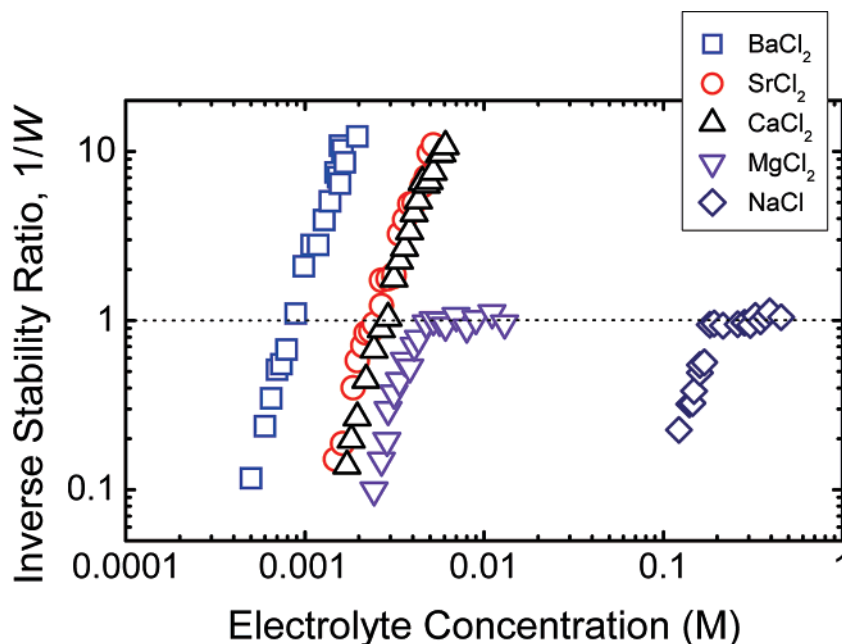


Figure 3. Inverse stability ratios of alginate-coated hematite nanoparticles as functions of monovalent and divalent electrolyte concentrations at pH 5.2. For all the aggregation experiments except the ones in the presence of NaCl and MgCl₂, the nanoparticle concentration employed is 7.5×10^7 particles/mL and the dissolved alginate concentration is $37.4 \mu\text{g/L}$. For the aggregation experiments in the presence of NaCl and MgCl₂, the nanoparticle concentration employed is 1.5×10^8 particles/mL and the dissolved alginate concentration is $74.8 \mu\text{g/L}$. The data obtained in the presence of NaCl, CaCl₂, and MgCl₂ were presented in our previous paper³⁰ and are included here for comparison purposes.

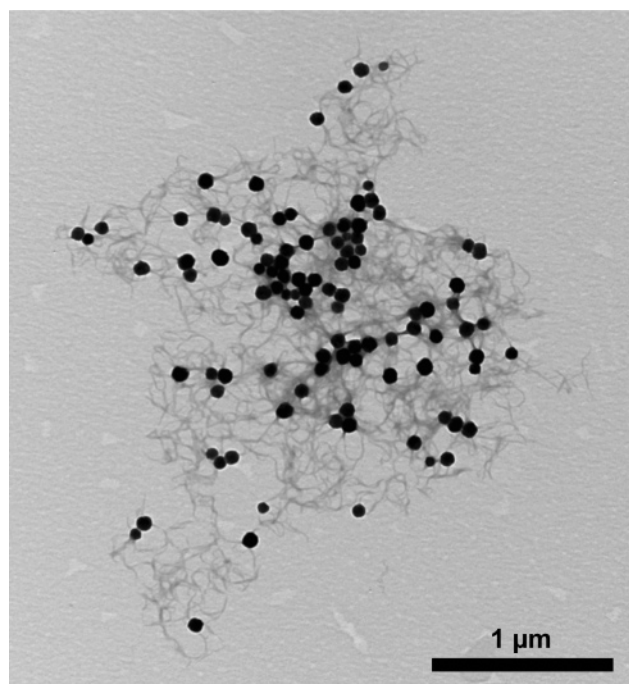


Figure 4. Combined hematite–alginate gel aggregate in the presence of 6 mM SrCl₂ at pH 5.2. Similar aggregate structures were found in the presence of 6 mM CaCl₂ and 2 mM BaCl₂. Aggregation was conducted at a particle concentration of 1.5×10^8 particles/mL and an adsorbed (dissolved) alginate concentration of $75 \mu\text{g/L}$. TEM images were captured 3–4 h after the initiation of aggregation.

surface at multiple locations in the presence of deionized water adjusted to pH 5.2. A representative approach force curve is presented in Figure 5. Repulsive electrostatic forces were consistently experienced from relatively long separation distances as the hematite-coated quartz substrate approached the hematite colloidal probe until contact occurred. From the approach force

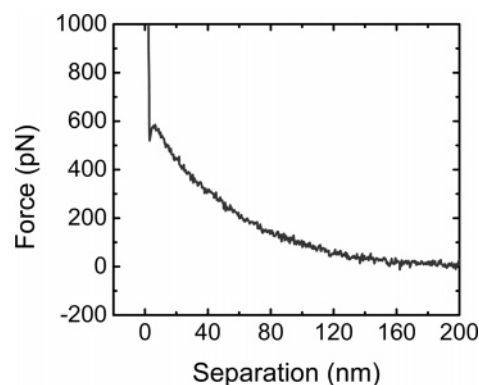


Figure 5. Representative approach force curve between the bare hematite colloidal probe and hematite-coated quartz surface in deionized water at pH 5.2, demonstrating the prevalence of long-range electrostatic repulsion.

profile, the characteristic decay length κ^{-1} was determined to be 53 nm using the method described by Byrd and Walz.⁴¹ This value corresponds to a theoretical Debye screening length for ionic strength conditions of 0.033 mM at a temperature of 25 °C. The experimentally determined κ^{-1} of 53 nm is reasonable as HCl was introduced into the deionized water to lower the pH to 5.2, thus slightly raising the solution ionic strength. This observation of repulsive forces between the probe and substrate at multiple locations established that the quartz surface was sufficiently coated with the hematite nanoparticles.

3.3.2. Adhesion Forces between Alginate-Coated Surfaces in the Presence of Sodium and Calcium Cations. Because alginate gel formation only occurs in the presence of CaCl₂ and not NaCl, a comparison of the retraction force interactions between alginate-coated hematite surfaces in both electrolytes can provide a better understanding of the physical properties of the alginate gel

(41) Byrd, T. L.; Walz, J. Y. *Environ. Sci. Technol.* **2005**, 39 (24), 9574–9582.

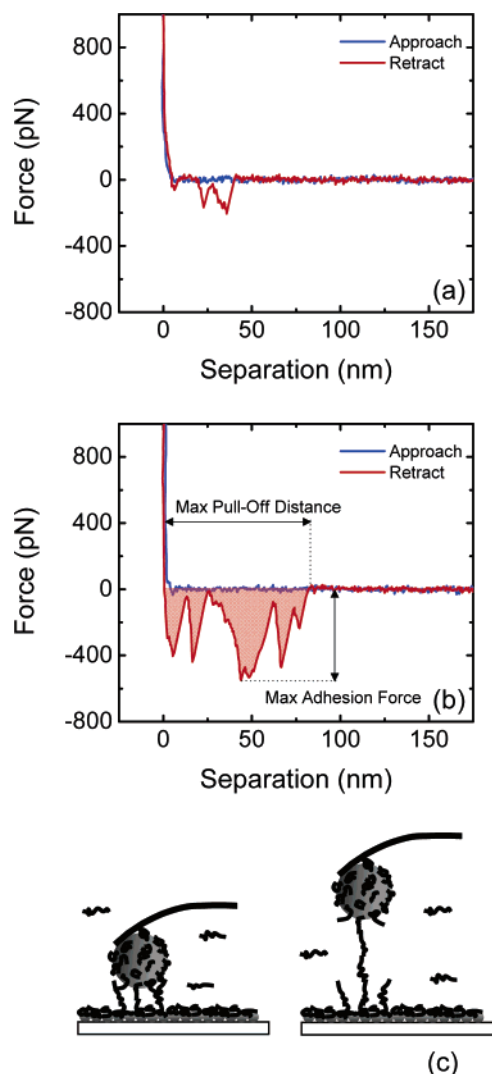


Figure 6. Representative force curves between alginate-coated hematite surfaces in the presence of (a) 200 mM NaCl and (b) 3 mM CaCl₂, both at pH 5.2. The maximum adhesion force, maximum pull-off distance, and work of adhesion (shaded area) are indicated in (b). (c) Illustration of alginate polymers bridging the hematite probe and substrate surface. As the substrate surface is retracted from the probe, some of the polymer bridges are broken and the probe pulls a chain made up of several alginate polymers from the substrate surface.

network that bridges hematite nanoparticles and thus results in the formation of the combined aggregates in the presence of CaCl₂. Representative force profiles between the alginate-coated hematite surfaces as the substrate was approached and retracted from the probe after contact in the presence of 200 mM NaCl are shown in Figure 6a. Note that this NaCl concentration is higher than the CCC of the alginate-coated hematite nanoparticles (section 3.2). At these conditions, the negative charges on both alginate layers are well screened. The maximum adhesion force between the layers was relatively small at approximately 200 pN and is likely contributed by van der Waals attraction and hydrogen bonding between the alginate polymers adsorbed on both the probe and substrate.⁴² The small pull-off distances indicated by the discontinuities (separation distances where peak forces occur) at about 23 and 36 nm were most likely a result of pulling off single alginate polymers as intermolecular bridging does not occur with NaCl.

In comparison, Figure 6b illustrates representative force profiles between the alginate-coated hematite surfaces in the presence of 3 mM CaCl₂ at pH 5.2. At this concentration, the inverse stability ratio $1/W$ approaches 1.8 (Figure 3), indicating enhanced aggregation of the alginate-coated hematite nanoparticles. Three major differences are observed when the retraction force profile in the presence of 3 mM CaCl₂ is compared with that in the presence of 200 mM NaCl. First, the maximum adhesion force is noticeably larger at about 550 pN in the presence of 3 mM CaCl₂. In CaCl₂ solutions, alginate polymers adsorbed on the probe and substrate are able to form bridges upon contact. This specific interaction is clearly stronger than the attraction due to van der Waals interaction and possibly hydrogen bonding in the presence of 200 mM NaCl. Second, more alginate polymers were pulled off during the retraction of the substrate from the probe in the presence of CaCl₂, as indicated by the numerous discontinuities (peaks) in the force profile (at separation distances of 6, 16, 49, 67, and 77 nm). Since alginate polymers bind more strongly through calcium complexation, the likelihood of pulling off a greater number of alginate polymers with each retraction is higher (illustrated in Figure 6c). The third difference between parts a and b of Figure 6 is the longer maximum pull-off distance in the presence of 3 mM CaCl₂. This strongly implies that, other than pulling off individual alginate polymers, each retraction might also lead to the stripping of chains of alginate polymers. These alginate polymers may be interlinked to form even longer chains of polymers through calcium bridging (illustrated in Figure 6c). Occasionally, we observed longer maximum pull-off distances associated with reduced maximum adhesion forces, as also noted for other polymer–substrate systems.⁴³ Nevertheless, the combination of the increasing maximum adhesion forces and pull-off distances results in a larger work of adhesion in the presence of 3 mM CaCl₂. This work of adhesion is defined as the work required to pull the alginate-coated surfaces apart.⁴³ As a first approximation, we calculated the work of adhesion by integrating the total area under the force profiles (shaded region in Figure 6b). This is a more holistic indicator of the alginate gelation propensity because it takes the adhesion force profile across the entire pull-off distance until the alginate polymers/chains break or are released from the surfaces. Comparing the retraction force profiles in Figure 6, the work of adhesion in the presence of 3 mM CaCl₂ is approximately 10 times that in 200 mM NaCl.

It is noted that negligible to small repulsive interaction forces were observed during the approach of the alginate-coated surfaces under the solution chemistries employed for the AFM measurements in this study (100 and 200 mM for NaCl and 1 and 3 mM for all divalent electrolytes). The approach force profiles shown in Figure 6 are also representative for all other solution chemistries employed for this study.

3.3.3. Comparing Maximum Adhesion Forces, Maximum Pull-Off Distances, and the Work of Adhesion. The average maximum adhesion forces, maximum pull-off distances, and work of adhesion in retracting the alginate-coated substrate from the alginate-coated probe in the various electrolytes are presented in Figure 7. These three indicators serve as the basis for comparisons of the strength of the alginate gel bridges in the presence of the different divalent cations. Measurements in the presence of the divalent electrolytes were conducted at the same concentrations of 1 and 3 mM for proper comparison. The measurements in the presence of 100 and 200 mM NaCl are also included as a reference, as the former concentration allows for

(42) de Kerchove, A. J.; Elimelech, M. *Macromolecules* **2006**, *39* (19), 6558–6564.

(43) Pericet-Camara, R.; Papastavrou, G.; Behrens, S. H.; Helm, C. A.; Borkovec, M. *J. Colloid Interface Sci.* **2006**, *296* (2), 496–506.

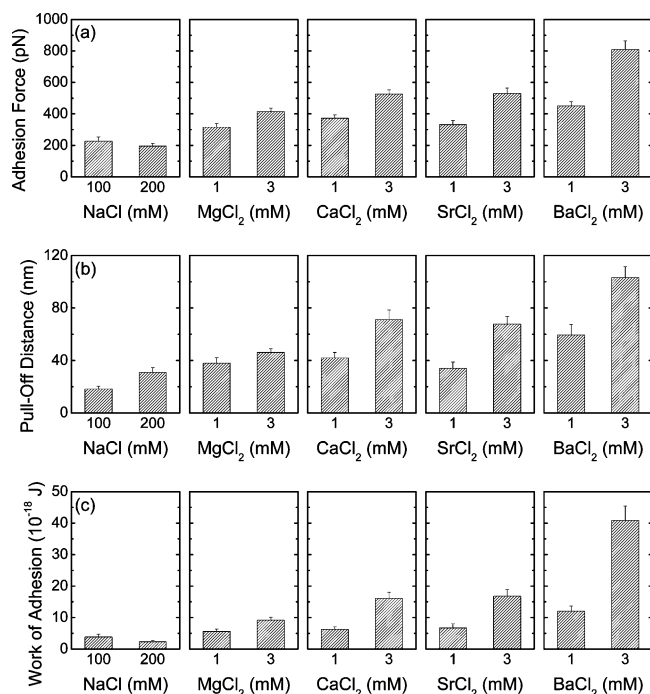


Figure 7. (a) Maximum adhesion forces between alginate-coated hematite surfaces at various concentrations of monovalent and divalent electrolytes at pH 5.2. (b) Maximum pull-off distances between alginate-coated hematite surfaces at various concentrations of monovalent and divalent electrolytes at pH 5.2. (c) Work of adhesion at various concentrations of monovalent and divalent electrolytes at pH 5.2. Average values of at least 100 measurements over 5–6 different locations on the substrate are presented. Error bars represent standard errors.

reaction-limited aggregation and the latter for diffusion-limited aggregation of the alginate-coated hematite nanoparticles.

In the presence of NaCl, alginate polymers do not undergo bridging, which explains the low values for all three indicators at both 100 and 200 mM. Since Mg²⁺ also does not participate in inter-polymer bridging of alginate, the three indicators have relatively low values at both 1 and 3 mM. However, in the presence of MgCl₂, the indicators have higher values than in NaCl, probably due to more efficient charge shielding of the alginate functional groups.

With CaCl₂ and SrCl₂, we observe that all three indicators have similar values at 1 and 3 mM, which is expected since we observed almost identical inverse stability profiles for these two electrolytes in the aggregation study (Figure 3). At 1 mM CaCl₂ and SrCl₂, the indicators are comparable to those in the case of NaCl and MgCl₂, probably because no significant alginate polymer bridging is likely to have occurred at such low concentrations. It is interesting to note that these conditions (i.e., 1 mM CaCl₂ and SrCl₂) do not lead to enhanced aggregation, i.e., $1/W < 1$ (Figure 3). However, at 3 mM CaCl₂ and SrCl₂, where $1/W > 1$, the indicators yield values larger than in NaCl and MgCl₂ due to bridging between the alginate polymers on the substrate and probe. This is especially noticeable when the work of adhesion is compared between the different electrolytes.

In the presence of 1 and 3 mM BaCl₂, the values of the three indicators are considerably greater than in the respective concentrations of CaCl₂ and SrCl₂. Once again, this observation is especially obvious when the work of adhesion is compared. The much larger values of the three indicators in the presence of BaCl₂ indicate that alginate has higher affinity for Ba²⁺, which leads to a higher degree of complexation compared to that of either Ca²⁺ or Sr²⁺. The higher affinity of alginate for Ba²⁺

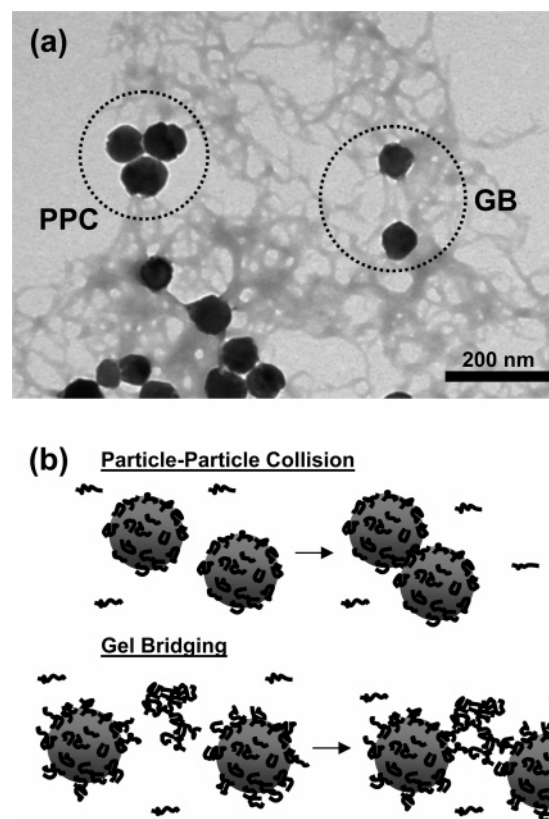


Figure 8. (a) Representative TEM image of the alginate-coated hematite colloids aggregated in the presence of 2 mM BaCl₂ at pH 5.2. The TEM image was captured 3–4 h after the initiation of aggregation. The hematite nanoparticle concentration is 1.5×10^8 particles/mL, and the dissolved alginate content is 75 μ g/L. The circled regions represent closed and open clusters resulting from PPC and GB, respectively. (b) At low Ca²⁺, Sr²⁺, or Ba²⁺ concentrations, the particle–particle collision mechanism dominates aggregation. At higher Ca²⁺, Sr²⁺, or Ba²⁺ concentrations, the gel bridging mechanism dominates and results in enhanced aggregation of alginate-coated hematite nanoparticles. The schematics are not drawn to scale and are for illustrative purposes only.

allows more efficient (faster) and stronger alginate inter-polymer bridging between the hematite surfaces. The behavior of the three indicators with Ba²⁺ agrees very well with our aggregation kinetics results that show that a much lower concentration of BaCl₂, compared to CaCl₂ and SrCl₂, is required to achieve a similar degree of enhanced aggregation.

3.4. Proposed Mechanism for Enhanced Aggregation with Ca²⁺, Sr²⁺, and Ba²⁺. Figure 8a presents a close-up TEM image of a combined hematite–alginate gel aggregate structure in the presence of 2 mM BaCl₂. This image is also representative of the structures observed in the presence of CaCl₂ and SrCl₂ at concentrations sufficient for enhanced aggregation of the alginate-coated hematite nanoparticles to occur. Upon closer inspection, we observe that, within the combined aggregate structure, primary hematite particles are either found in direct contact, forming doublets or lower-order aggregates, or held together by the alginate gel network as singlets. Therefore, we propose two aggregation mechanisms of the alginate-coated hematite nanoparticles that take place simultaneously in the presence of CaCl₂, SrCl₂, and BaCl₂, both illustrated in Figure 8b.

The first mechanism occurs through particle–particle collision (PPC). Even in the presence of a low concentration of divalent cations, the adsorbed alginate polymers are able to fold and collapse onto the hematite nanoparticle surface due to complexation of the divalent cations, resulting in charge neutralization

of the negatively charged alginate functional groups.³⁰ In this case, the nanoparticles no longer experience electrosteric repulsion and come to a permanent attachment after collision. This mechanism is similar to any conventional aggregation process controlled by electrostatic and van der Waals interactions between colloidal particles and does not lead to enhanced aggregation. This is likely to be the sole aggregation mechanism for the alginate-coated hematite nanoparticles in the presence of NaCl and MgCl₂.

The second mechanism is gel bridging (GB). In the presence of Ca²⁺, Sr²⁺, and Ba²⁺ cations, dissolved alginate polymers also undergo bridging when they diffuse into contact to form alginate gel clusters. It is possible that dissolved alginate polymers may also undergo bridging with the alginate adsorbed on the hematite nanoparticles. The speed (efficiency) of gel formation and integrity of the gel formed may be dependent on the type and concentrations of divalent cations present, as shown in our DLS and AFM measurements. Eventually, the alginate gel clusters bridge the primary particles and lower-order aggregates together, resulting in the combined hematite–alginate gel aggregates. The presence of a divalent cation which alginate has a higher affinity for will allow for faster gel formation and lead to a greater degree of enhanced aggregation, as observed in the presence of Ba²⁺ cations. In other words, the mechanism of gel bridging is akin to heteroaggregation occurring within the binary system made up of nanoparticles (hematite) and polymers (alginate). This second mechanism of gel bridging is essential for enhanced aggregation and results in much larger aggregate formation in a relatively short time period.

4. Conclusion

The aggregation kinetics of alginate-coated hematite nanoparticles were determined over a wide range of concentrations of monovalent and divalent electrolytes. Enhanced aggregation

kinetics were observed at higher concentrations of Ca²⁺, Sr²⁺, and Ba²⁺, but not with Na⁺ and Mg²⁺ cations. To achieve similar enhanced aggregation kinetics, the divalent cation concentration required follows the order [Ca²⁺] > [Sr²⁺] ≫ [Ba²⁺]. TEM imaging of the aggregate structures formed under conditions favoring enhanced aggregation revealed an extended alginate gel that bridged hematite nanoparticles and lower-order aggregates together. AFM retraction force measurements between the alginate-coated hematite surfaces indicated the maximum adhesion forces, maximum pull-off distances, and work of adhesion to be larger when specific binding between the alginate polymers occurred in the presence of Ca²⁺, Sr²⁺, and Ba²⁺. In the presence of Na⁺ and Mg²⁺, the values of the three indicators were smaller because Na⁺ and Mg²⁺ lack specific interactions with alginate. In the presence of Ba²⁺, all three indicators had larger values when compared to those of either Ca²⁺ or Sr²⁺, which is consistent with the aggregation kinetics results. The observed behavior may be indicative of the alginate's affinity for the divalent cations. We hypothesize that enhanced aggregation occurs in the presence of sufficiently high concentrations of Ca²⁺, Sr²⁺, or Ba²⁺, as the dissolved (unadsorbed) alginate polymers undergo bridging to form alginate gel clusters, which subsequently bridge the hematite nanoparticles and aggregates together.

Acknowledgment. Funding was provided by the National Science Foundation (Grant BES 0504258). We acknowledge Dr. Seoktae Kang (Department of Chemical Engineering, Environmental Engineering Program, Yale University) for taking the SEM images in this study. The images of the hematite–alginate gel aggregates were captured with the transmission electron microscope in the Department of Cell Biology of the Yale University School of Medicine.

LA063744K